Article DOI: https://doi.org/10.3201/eid3212.251211

EID cannot ensure accessibility for supplementary materials supplied by authors. Readers who have difficulty accessing supplementary content should contact the authors for assistance.

Mayaro Virus Emergence and Genetic Dynamics, Peru

Appendix

Additional Methods

Ethics Statement and Informed consent

Ethical approval for this study was granted through the Ethical Review Committee (SIDISI 210258, March 2023) from Universidad Peruana Cayetano Heredia, Lima, Peru with yearly extensions.

Samples

The sampling timeframe for this study consisted of patients presenting with acute febrile illness at six participating health facilities in Peru between September 2023 and October 2024. Whole blood and plasma specimens were collected from 1 000 patients consenting as part of a facility-based clinical surveillance and pathogen-detection effort, designed to investigate causes of acute febrile illness. The rationale for including these specimens was that Mayaro virus infection can present as a non-specific, febrile illness that overlaps clinically with other arboviral and viral infections, making molecular screening and genomic characterization useful for detecting otherwise unrecognized circulation. This sampling strategy was not designed as a population-based prevalence survey. Instead, the study population represents symptomatic, healthcare-seeking individuals encountered at participating facilities.

Total Nucleic Acid Extraction and cDNA Synthesis

Total nucleic acids (TNA) were extracted from 400 µL of each whole blood specimen using the MagMAX MVP II kit (ThermoFisher Scientific, Waltham, MA) on a KingFisher Apex instrument, following a laboratory-optimized protocol. Extraction controls included positive controls (two viral stocks and one bacterial stock spiked into HIV-positive plasma at 3.0 log copies/mL) and negative controls (normal human blood and buffer-only). Subsequently, 10 µL

of extracted TNA was used for cDNA synthesis employing the SuperScript IV First-Strand Synthesis System for RT-PCR (Invitrogen, ThermoFisher Scientific) along with Sequenase v2.0 DNA Polymerase (Applied Biosystems, ThermoFisher Scientific). The resulting cDNA products were purified using AMPure XP PCR Cleanup beads (Beckman Coulter).

Library Preparation, Target Enrichment, and DNA Sequencing

NGS libraries were prepared using the Illumina Nextera XT Library Preparation Kit for 24 cycles with non-biotinylated, unique dual index barcode adapters (Integrated DNA Technologies) as recently described in Yamaguchi et al. (*1*). Libraries were purified with AMPure XP PCR cleanup beads (Beckman Coulter, California). Libraries were assessed for size and quality using a TapeStation 4200 (Agilent) and quantified using a Qubit Flex Fluorometer (ThermoFisher Scientific). Next, an aliquot of each metagenomic library, with a maximum of twenty-four libraries and 3,000 ng total, were pooled together for target enrichment. Pools were dried using a vacuum centrifuge, resuspended in a solution of human Cot-1 DNA and Universal Nextera Blockers (Integrated DNA Technologies), and hybridized to Comprehensive Viral Research Panel (CVRP, Twist Biosciences) probes for 16 hours per manufacturer instructions. Hybridized reads were captured by affinity interaction on streptavidin beads (Twist Biosciences), amplified using a KAPA library amplification kit (Roche), and re-purified using magnetic beads (Twist Biosciences). Viral-enriched libraries were analyzed for size and concentration as before. Equimolar mNGS and CVRP library pools were combined in 9:1 v/v ratio. Next-generation sequencing of of n = 48 teamNGS combined libraires was performed on an Illumina NextSeq instrument using a NextSeq p2 300 cycle flow cell. Raw FASTQ files were quality processed and de-hosted by removing human-derived reads before microbial classification as described by Yamaguchi et al. (*1*). Viral reads were then normalized as reads per million and evaluated by reference mapping in CLC Genomics Workbench to generate coverage metrics and consensus sequences.

Genomic Data Collection and Phylogenetic Analysis

We retrieved all sequences of MAYV available in NCBI Virus database repository (https://www.ncbi.nlm.nih.gov/labs/virus/vssi/#/) on February 6th, 2025. All downloaded sequences were visually inspected and selected those with complete or near complete sequences (genome>60% coverage). All sequence information including GenBank ID and metadata are available at https://github.com/LesterJP/MAYV_Peru. Sequences were aligned together with the

sequences obtained in the current study using MAFFT software v7.453 (*2*) with settings for a "*localpair*" option alignment. The alignments were then used for maximum likelihood (ML) phylogenetic inference using IQ-TREE2 (*3*) as described in Perez et al (*4*).

Recombination Screening and Confirmation

Searches for recombinant sequences and best-supported breakpoints were performed using the workflow previously applied in Perez et al. (*5*,*6*), with minor modifications. Recombination was screened in RDP5 v5 using seven methods: RDP, GENECONV, BootScan, MaxChi, Chimaera, SiScan, and 3Seq (*7*). Settings were adjusted according to RDP5 recommendations for divergent viral datasets. Preliminary recombinant candidates were defined as events detected by >3 methods with $p < 0.01$ after Bonferroni correction. Because RDP-based screening can generate false-positive signals, candidates were further confirmed using: 1) (Pairwise Homoplasy Index, test:PHI test evidence of recombination, 2) BootScan support >75%, and 3) phylogenetic incongruence across inferred recombinant and non-recombinant regions assessed by Shimodaira-Hasegawa topology tests (*7*). Only candidates satisfying these statistical, phylogenetic, and epidemiologic plausibility criteria were considered confirmed recombinants (*5*,*6*).

RDP5 identified six preliminary recombination signals in the MAYV dataset, including signals involving the previously reported putative recombinant strains HAITI15/KX496990 and 2BR14/KT818520 (*8*). However, none fulfilled the full confirmation criteria. The strongest candidate event, HAITI15/KX496990, lacked consistent downstream topology-based support, including non-significant support in the minor-parent region. The 2BR14/KT818520-associated signal was also not retained as a confirmed recombinant. Therefore, no MAYV genomes were excluded from the final phylogenetic, molecular-clock, or phylodynamic analyses as confirmed recombinants.

Temporal and Demographic Bayesian Inference

To determine the temporal emergence and evolutionary rate of MAYV globally and the strains circulating in Peru we used the methodology previously described in Redman et al. (*9*) with some modifications. We first evaluated the temporal signal for the dataset using the methodology described in Perez et al. (*5*) with some modifications: temporal signal, we used a Bayesian Evaluation of Temporal Signal framework (BETS) (*10*), in which heterochronous

analyses retaining the original sampling dates were compared with corresponding isochronous controls. Log marginal-likelihood estimators (log MLEs), specifically path sampling and stepping-stone sampling methods Marginal likelihoods were estimated using both path-sampling and stepping-stone sampling, and log Bayes factors were calculated for each clock/coalescent-prior combination. Prior distributions were set with an exponential mean of 1.0 for the clock and an exponential population size with a mean of 10.0 and an offset of 0.5 for the coalescent prior. MLE was obtained using path sampling and stepping-stone sampling, with a chain length of 9×10^6 and 900 path steps. These analyses supported sufficient temporal signal in the dataset, with heterochronous models favored over their corresponding isochronous controls (Appendix Table 1), The strongest support was obtained for the uncorrelated relaxed molecular clock combined with the GMRF Bayesian Skyride coalescent prior, with log Bayes factors of 1495.36 using path-sampling and 1461.68 using stepping-stone sampling. This clock/prior combination was therefore selected for the final time-scaled phylogenetic inference (Appendix Table 1). Time-scaled phylogenies were generated using BEAST 1.10.5 (*11*) with the BEAGLE 3 library (*12*) employed to enhance computational efficiency. Molecular clock parameters used here were previously described in Perez et al (*6*). In addition, a Skydride tree prior model (*13*) was selected for the analysis. Four independent runs were executed, each sampling from the Markov Chain Monte Carlo (MCMC) chains at intervals of $9x10^8$ generations with sampling every $9x10^5$ generations. Subsequent evaluation of convergence was determined by the effective sample size (ESS) parameter estimates, with values of ESS >200 determined using Tracer 1.7 software (*8*).

Discrete and Continues Phylogeographic Analysis

To infer the geographic dynamics of MAYV and identify sources of external introductions and local lineage emergence in Peru, we first performed discrete trait phylogeographic analysis following Perez et al. (*4*,*5*). Next, to evaluate the local spread of the two main lineages identified by Phylowave (*14*), we partitioned the dataset and conducted separate continuous phylogeographic analyses in BEAST v1.10.4 (*15*) using the selected relaxed molecular clock and Skyride coalescent prior. Continuous phylogeographic reconstruction was performed using a relaxed random-walk diffusion model with a gamma distribution to account for among-branch variability in diffusion rates. Locations were converted into latitude and longitude coordinates at the most precise administrative level available (Appendix Table 2) (*16*,*17*). Spatial jittering was applied using a jitter window of 0.01 to reduce artificial clustering

of sequences assigned to identical or near-identical coordinates. Two independent MCMC runs were performed for each lineage, each for 9×10^8 generations and sampled every 9×10^5 generations (*16*). Convergence was assessed in Tracer v1.7, and all relevant parameters reached ESS >200. Maximum clade credibility trees were summarized using TreeAnnotator v1.10. *Post hoc* spatiotemporal analyses were performed using the R package Seraphim 2.0 (*18*) to extract dispersal metrics from posterior trees.

Lineage Emergence and Evolutionary Fitness

To investigate the emergence of distinct MAYV lineages and assess their evolutionary fitness, we employed the novel Phylowave approach (*14*). Phylowave efficiently summarizes changes in population composition within phylogenetic trees, automatically detecting lineages based on shared fitness characteristics. For this analysis, we used the maximum clade credibility (MCC) tree derived from our temporal analysis as input and executed the Phylowave scripts available on the GitHub repository: https://github.com/noemielefrancq/Phylowave_Learning-fitness-dynamics-pathogens-in-phylogenies/tree/v).

Design and Development of a Novel Dual Target RT-qPCR for MAYV

Previously reported MAYV RT-qPCR assays, including those described by Naveca et al (*19*)., Waggoner et al. (*20*), and Wesselmann et al. (*21*), were evaluated in silico by aligning their primer/probe binding regions against available MAYV genomic diversity. This analysis identified mismatches in several primer/probe regions across representative sequences and lineages, supporting the design of an updated assay with improved sequence inclusivity. Primer and probe sets for the specific detection of MAYV were selected following the methodology described by Perez et al. (*22*). Briefly, using all available sequences (Appendix Table 1 at Github repository: https://github.com/LesterJP/MAYV_Peru), regions of lower variability were selected based on Shannon entropy analysis. Primers and probes were designed using Oligo 7.6 software (Molecular Biology Insights, United States) with selection parameters set to optimize priming efficiency in a TaqMan assay (*23*,*24*). *In silico* evaluations for specificity were performed using the GenBank nucleotide database and BLASTn searches. RT-qPCR experiments were conducted on an *m*2000rt Real-Time PCR System instrument (Abbott Molecular, Des Plaines, IL, United States), and results were analyzed using MultiAnalyze software. Serial dilutions of in vitro transcripts in nuclease-free water were tested with the respective primer/probe sets to determine linearity and efficiency. Similarly, the analytical sensitivity (ASe) was estimated by evaluating

ten-fold serial dilutions of quantified RNA transcript standards, determined using a Probit regression analysis implemented in MedCalc Statistical Software version 19.0.7 (MedCalc Software bvba, Ostend, Belgium; 2019). The ASe was defined as the concentration (copies of transcripts per reaction) that yielded 95% positive results along with a 95% Confidence Interval (CI) (*22*). Finally, a Research Use Only (RUO) assay for the automated *m*2000 platform (Abbott Molecular, Des Plaines, IL) was developed following the chemistry conditions and addition of an internal control as described in Anderson et al. (*25*).

References

1. Yamaguchi J, Orf GS, Malinauskas J, Mata M, Weiss SL, Forberg K, et al. teamNGS balances sensitivity for viruses with comprehensive microbial detection in clinical specimens. Microorganisms. 2025;13:2854. PubMed https://doi.org/10.3390/microorganisms13122854

2. Rozewicki J, Li S, Amada KM, Standley DM, Katoh K. MAFFT-DASH: integrated protein sequence and structural alignment. Nucleic Acids Res. 2019;47(W1):W5–10. PubMed https://doi.org/10.1093/nar/gkz342

3. Nguyen LT, Schmidt HA, von Haeseler A, Minh BQ. IQ-TREE: a fast and effective stochastic algorithm for estimating maximum-likelihood phylogenies. Mol Biol Evol. 2015;32:268–74. PubMed https://doi.org/10.1093/molbev/msu300

4. Perez LJ, Orf GS, Berg MG, Rodgers MA, Meyer TV, Mohaimani A, et al. The early SARS-CoV-2 epidemic in Senegal was driven by the local emergence of B.1.416 and the introduction of B.1.1.420 from Europe. Virus Evol. 2022;8:veac025. PubMed https://doi.org/10.1093/ve/veac025

5. Pérez LJ, Baele G, Hong SL, Cloherty GA, Berg MG. Ecological changes exacerbating the spread of invasive ticks has driven the dispersal of severe fever with thrombocytopenia syndrome virus throughout Southeast Asia. Mol Biol Evol. 2024;41:msae173. PubMed https://doi.org/10.1093/molbev/msae173

6. Perez LJ, Forberg K, Cloherty GA, Berg MG. Temporal and coevolutionary analyses reveal the events driving the emergence and circulation of human mamastroviruses. Emerg Microbes Infect. 2023;12:2217942. PubMed https://doi.org/10.1080/22221751.2023.2217942

7. Martin DP, Varsani A, Roumagnac P, Botha G, Maslamoney S, Schwab T, et al. RDP5: a computer program for analyzing recombination in, and removing signals of recombination from, nucleotide sequence datasets. Virus Evol. 2020;7:veaa087. PubMed https://doi.org/10.1093/ve/veaa087

8. Mavian C, Rife BD, Dollar JJ, Cella E, Ciccozzi M, Prosperi MCF, et al. Emergence of recombinant Mayaro virus strains from the Amazon basin. Sci Rep. 2017;7:8718. PubMed https://doi.org/10.1038/s41598-017-07152-5

9. Redman SA, Perez LJ, Forberg K, Francis K, Walker JP, Thompson TK, et al. Dengue virus serotype 3 origins and genetic dynamics, Jamaica. Emerg Infect Dis. 2024;30:2149–54. PubMed https://doi.org/10.3201/eid3010.240170

10. Duchene S, Lemey P, Stadler T, Ho SYW, Duchene DA, Dhanasekaran V, et al. Bayesian evaluation of temporal signal in measurably evolving populations. Mol Biol Evol. 2020;37:3363–79. PubMed https://doi.org/10.1093/molbev/msaa163

11. Suchard MA, Lemey P, Baele G, Ayres DL, Drummond AJ, Rambaut A. Bayesian phylogenetic and phylodynamic data integration using BEAST 1.10. Virus Evol. 2018;4:vey016. PubMed https://doi.org/10.1093/ve/vey016

12. Ayres DL, Cummings MP, Baele G, Darling AE, Lewis PO, Swofford DL, et al. BEAGLE 3: improved performance, scaling, and usability for a high-performance computing library for statistical phylogenetics. Syst Biol. 2019;68:1052–61. PubMed https://doi.org/10.1093/sysbio/syz020

13. Hill V, Baele G. Bayesian estimation of past population dynamics in BEAST 1.10 using the Skygrid coalescent model. Mol Biol Evol. 2019;36:2620–8. PubMed https://doi.org/10.1093/molbev/msz172

14. Lefrancq N, Duret L, Bouchez V, Brisse S, Parkhill J, Salje H. Learning the fitness dynamics of pathogens from phylogenies. Nature. 2025;637:683–90. PubMed https://doi.org/10.1038/s41586-024-08309-9

15. Suchard MA, Lemey P, Baele G, Ayres DL, Drummond AJ, Rambaut A. Bayesian phylogenetic and phylodynamic data integration using BEAST 1.10. Virus Evol. 2018;4:vey016. PubMed https://doi.org/10.1093/ve/vey016

16. Dellicour S, Gill MS, Faria NR, Rambaut A, Pybus OG, Suchard MA, et al. Relax, keep walking—a practical guide to continuous phylogeographic inference with BEAST. Mol Biol Evol. 2021;38:3486–93. PubMed https://doi.org/10.1093/molbev/msab031

17. Lemey P, Rambaut A, Welch JJ, Suchard MA. Phylogeography takes a relaxed random walk in continuous space and time. Mol Biol Evol. 2010;27:1877–85. PubMed https://doi.org/10.1093/molbev/msq067

18. Dellicour S, Faria NR, Rose R, Lemey P, Pybus OG. SERAPHIM 2.0: an extended toolbox for studying phylogenetically informed movements. Bioinformatics. 2026;42:btag093. PubMed https://doi.org/10.1093/bioinformatics/btag093

19. Naveca FG, Nascimento VAD, Souza VC, Nunes BTD, Rodrigues DSG, Vasconcelos PFDC. Multiplexed reverse transcription real-time polymerase chain reaction for simultaneous detection of Mayaro, Oropouche, and Oropouche-like viruses. Mem Inst Oswaldo Cruz. 2017;112:510–3. PubMed https://doi.org/10.1590/0074-02760160062

20. Waggoner JJ, Rojas A, Mohamed-Hadley A, de Guillén YA, Pinsky BA. Real-time RT-PCR for Mayaro virus detection in plasma and urine. J Clin Virol. 2018;98:1–4. PubMed https://doi.org/10.1016/j.jcv.2017.11.006

21. Wesselmann KM, Baronti C, Nougairède A, Thirion L, de Lamballerie X, Charrel R, et al. Development and evaluation of a duplex RT-qPCR assay for the detection and identification of Mayaro and chikungunya viruses. J Clin Microbiol. 2025;63:e0042025. PubMed https://doi.org/10.1128/jcm.00420-25

22. Pérez LJ, Lanka S, DeShambo VJ, Fredrickson RL, Maddox CW. A Validated multiplex real-time PCR assay for the diagnosis of infectious *Leptospira* spp.: a novel assay for the detection and differentiation of strains from both pathogenic groups I and II. Front Microbiol. 2020;11:457. PubMed https://doi.org/10.3389/fmicb.2020.00457

23. Rios L, Perera CL, Coronado L, Relova D, Álvarez AM, Ganges L, et al. Multi-target strategy for pan/foot-and-mouth disease virus (FMDV) detection: a combination of sequences analysis, *in silico* predictions and laboratory diagnostic evaluation. Front Vet Sci. 2018;5:160. PubMed https://doi.org/10.3389/fvets.2018.00160

24. Acevedo AM, Perera CL, Vega A, Ríos L, Coronado L, Relova D, et al. A duplex SYBR Green I-based real-time RT-PCR assay for the simultaneous detection and differentiation of Massachusetts and non-Massachusetts serotypes of infectious bronchitis virus. Mol Cell Probes. 2013;27:184–92. PubMed https://doi.org/10.1016/j.mcp.2013.06.001

25. Anderson M, Hodges A, Luk KC, Olivo A, Forberg K, Meyer TV, et al. Development and validation of three automated high-throughput molecular tests to detect monkeypox virus infections. J Infect Dis. 2024;229(Supplement_2):S137–43. PubMed https://doi.org/10.1093/infdis/jiad406

Appendix Table 1. Assessment of temporal signals and combination of molecular clock model and demographic prior using BETS analysis*

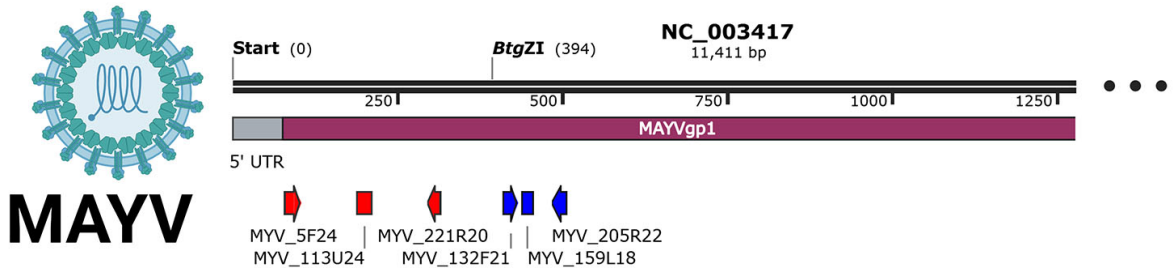
	Heterochronous		Isochronous				
Clock model and coalescent	Path Sampling (PS)	Stepping Stone (SS)	Path Sampling (PS)	Stepping Stone (SS)	log Bayes factor (PS)	log Bayes factor (SS)	Temporal signal
Strict							
Constant	−48124.12796	−48124.99445	−48249.03922	−48244.24769	124.9112653	119.2532468	yes
Exponential	−48126.14002	−48123.19071	−48248.98879	−48243.34183	122.8487657	120.1511213	yes
Bayesian Skyline Plot	−48117.64236	−48119.7049	−48239.79825	−48240.61741	122.1558929	120.9125167	yes
Bayesian skygrid	−48124.7505	−48123.89383	−48355.87657	−48340.00863	231.1260774	216.1147936	yes
Bayesian Skyride (GMRF)	−48169.50328	−48167.1371	−48493.20061	−48473.81623	323.6973312	306.6791316	yes
Uncorelated relaxed local							
Constant	−47447.9729	−47447.33556	−47452.21882	−47453.27924	4.245922441	5.943674799	yes
Exponential	−47473.32785	−47469.63518	−48255.43041	−48244.8365	782.1025562	775.2013173	yes
Bayesian Skyline Plot	−47449.04444	−47452.69941	−47449.22245	−47453.16302	0.178012307	0.463608741	yes
Bayesian skygrid	−47441.55597	−47429.87706	−48196.64679	−48165.56726	755.0908236	735.6902007	yes
Bayesian Skyride (GMRF)	−47456.17007	−47455.1267	−48944.40035	−48914.83932	1495.355909	1461.6763	yes

*Log marginal likelihood values obtained through path sampling and stepping-stone sampling methods. The presence of a temporal signal was quantified by the log Bayes factor, calculated from the difference in log marginal likelihoods between the heterochronous model (incorporating sampling dates) and the isochronous model (excluding sampling dates).

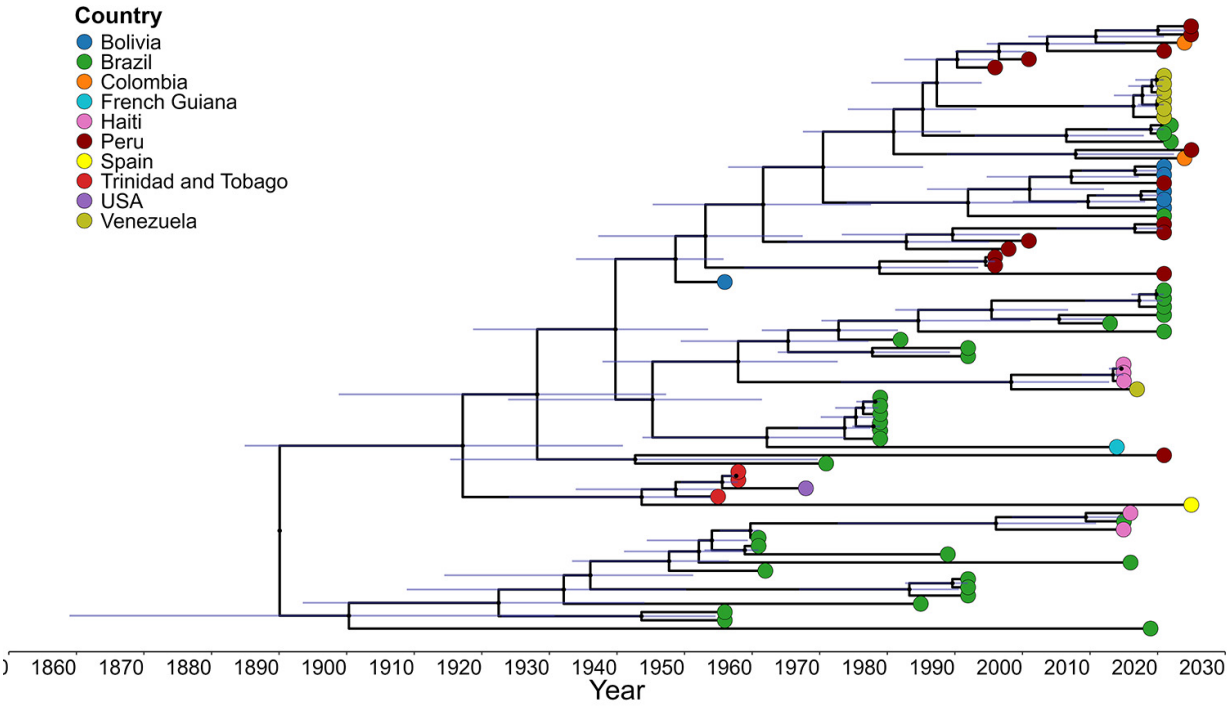
Appendix Table 2. GenBank accession, geographic locations and lineages assignments for Mayaro virus sequences included in the continuous phylogeographic analysis*

ID	Latitude	Longitude	Lineage
KP842800	−9.189967	−75.015152	2
KP842801	−9.189967	−75.015152	2
KP842802	−14.235	−51.9253	2
KP842803	−14.235	−51.9253	2
KP842804	−14.235	−51.9253	2
MK573241	−14.235	−51.9253	2
MK573242	−9.189967	−75.015152	2
MK573244	−14.235	−51.9253	2
MK573246	−16.2902	−63.5887	2
KY618139	−14.235	−51.9253	2
KJ013266	4.9224	−52.3135	2
KY618136	−14.235	−51.9253	2
KY618137	−14.235	−51.9253	2
KY618138	−14.235	−51.9253	2
KY618128	−14.235	−51.9253	2
KY618132	−14.235	−51.9253	2
KY618131	−14.235	−51.9253	2
MK837006	18.5392	−72.336	2
MK837007	18.5392	−72.336	2
MN138459	18.5392	−72.336	2
MK288026	7	−66	2
KY618140	−14.235	−51.9253	2
KY618134	−14.235	−51.9253	2
KY618130	−14.235	−51.9253	2
APDC070024	−9.189967	−75.015152	3
APDC070034	−9.189967	−75.015152	3
APDC060121	−9.189967	−75.015152	3
PP339762	−14.235	−51.9253	3
PP339763	−14.235	−51.9253	3
PP339764	−14.235	−51.9253	3
KP842815	−9.189967	−75.015152	3
KP842816	−9.189967	−75.015152	3
KP842817	−16.2902	−63.5887	3
KP842794	7	−66	3
KP842795	7	−66	3
KP842796	7	−66	3
KP842797	7	−66	3
KP842798	7	−66	3
KP842799	7	−66	3
KP842805	−16.2902	−63.5887	3
KP842806	−16.2902	−63.5887	3
KP842807	−9.189967	−75.015152	3
KP842808	−9.189967	−75.015152	3
KP842811	−9.189967	−75.015152	3
KP842813	−9.189967	−75.015152	3
KP842814	−16.2902	−63.5887	3
PP505832	4.5709	−74.2973	3
PP505831	4.5709	−74.2973	3
MK573243	−9.189967	−75.015152	3
MK573245	−16.2902	−63.5887	3
KM400591	−14.235	−51.9253	3
MK070491	−9.189967	−75.015152	3

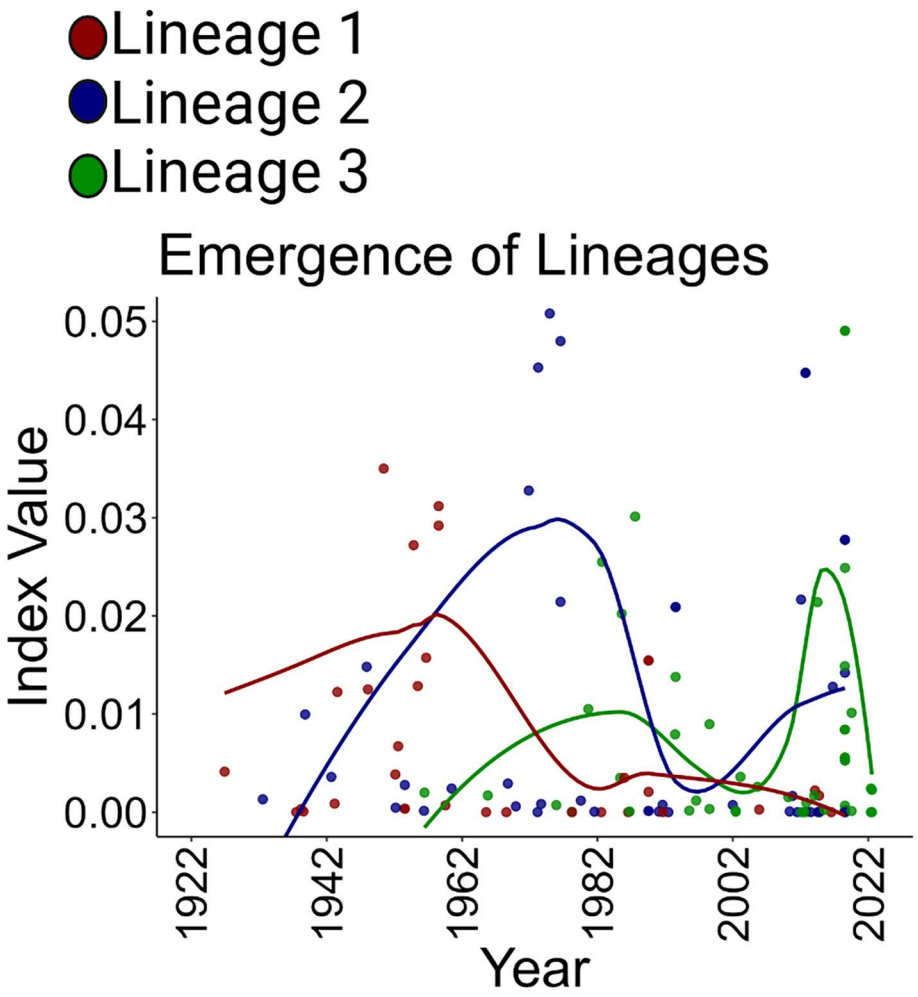
*Coordinates were extracted directly from the corresponding GenBank annotations and were not assigned as regional centroid in the study.



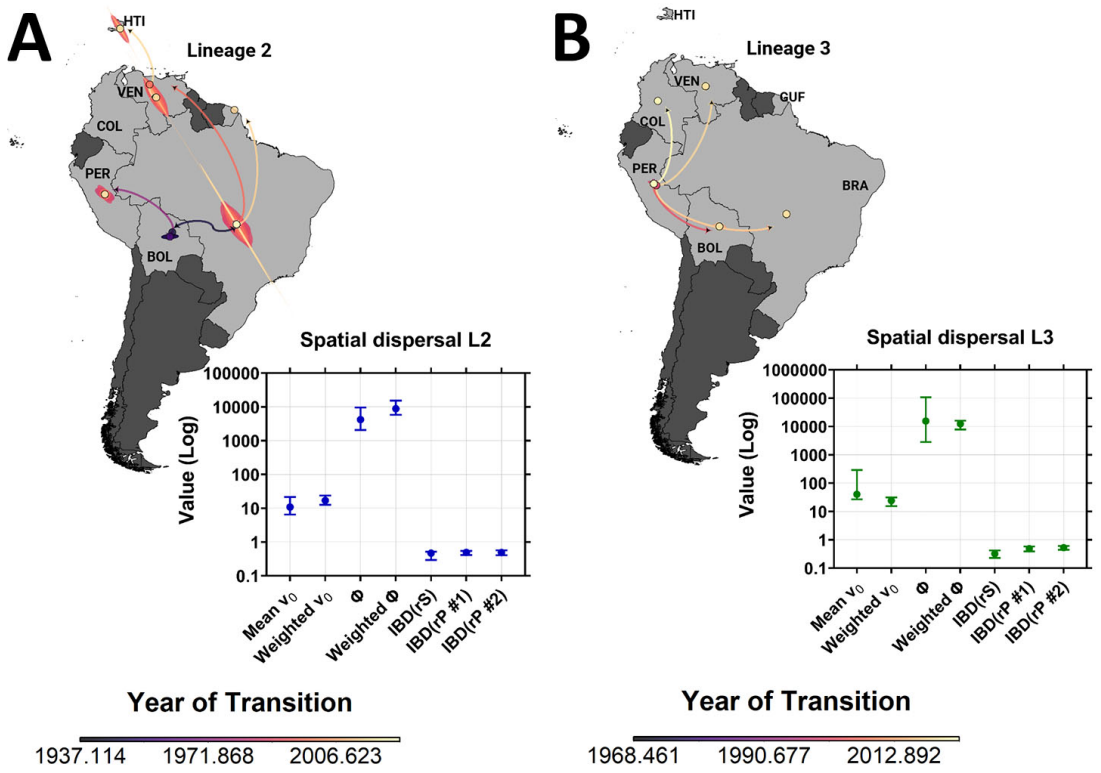
Appendix Figure 1. Target regions selected for the Mayaro virus dual-target assay. Schematic representation of the Mayaro virus (MAYV) genomic region used for dual-target assay design, mapped to the reference genome NC_003417. The two primer-probe sets target distinct regions within the MAYVgp1 coding sequence: MYV_5F24, MYV_113U24, and MYV_132F21, and MYV_221R20, MYV_159L18, and MYV_205R22.



Appendix Figure 2. Time-scaled MCC phylogeny of Mayaro virus with 95% HPD intervals. Maximum clade credibility tree showing the temporal structure of the MAYV dataset used for phylodynamic analyses. Branches are scaled in calendar time, and tips are colored according to the country of sampling. Horizontal blue bars represent the 95% highest posterior density intervals for node ages across all internal nodes, and black node points indicate the median estimated node age. The x-axis represents calendar year. This supplementary tree provides the full visualization of node-age uncertainty supporting the time-scaled phylogeny shown in



Appendix Figure 3. Temporal dynamics and emergence of Mayaro virus lineages inferred using PhyloWave. Lineage-specific index values were calculated at each terminal and internal node to track changes in lineage composition over time. Individual points represent node-level index values, while fitted curves illustrate the temporal dynamics of Lineage 1 (red), Lineage 2 (blue), and Lineage 3 (green).



Appendix Figure 4. Reconstructed spatial dispersal histories of Mayaro virus lineages 2 and 3. Continuous phylogeographic reconstructions depict the inferred dispersal of lineage 2 (A) and lineage 3 (B) across Central and South America, as defined by the lineage index-dynamics analysis. Dispersal trajectories are colored according to the estimated year of transition, with corresponding temporal scales shown below each map. Geographic nodes indicate inferred ancestral and sampled locations, and branches represent transitions among locations. The plots summarize lineage-specific spatial diffusion metrics, including mean and weighted dispersal velocities (v, km/year), mean and weighted diffusion coefficients (D, km^2/year), and isolation-by-distance correlations (IBD, Pearson's *r*). Points represent estimated values, and error bars denote the corresponding uncertainty intervals.